Journal of Sound and Vibration (1999) **224**(4), 757–774
Article No. jsvi.1999.2207, available online at http://www.idealibrary.com on IDEAL®

PREDICTION OF POWER FLOWS THROUGH MACHINE VIBRATION ISOLATORS

W. L. Li and P. Lavrich

United Technologies Carrier Corporation, Carrier Parkway, Syracuse, NY 13221, *USA*

(*Received* 2 *October* 1998; *and in final form* 19 *February* 1999)

A dynamic model is described for vibration isolation systems consisting of a source machine, multiple vibration isolators and a supporting structure. The machine is modeled as a rigid body of six degrees of freedom. Each of the isolators is treated as an assembly of six simple translational and rotational springs and allowed to be inclined at arbitrary angles. The supporting structure is composed of a rectangular plate and a number of reinforcing beams placed in any directions. The equation of motion of such a composite structure is derived from Hamilton's principle and then combined with that of the machine to determine the modal characteristics and vibrations of the whole isolation system, the reaction forces at each isolator, and the power flows into the supporting structure. Numerical examples are presented to examine the power flows under various situations.

1. INTRODUCTION

A vibratory machine such as an engine or a compressor is often mounted *via* vibration isolators onto a supporting structure, as a common practice for noise and vibration control. Usually, in a vibration isolation analysis only the machine and isolators are explicitly considered by assuming that the supporting structure has a much larger impedance than the isolators do. As a result, the reaction forces or force transmissibilities are often used to measure the performance of an isolation system. Since the reaction forces at each mounting point are typically different in both amplitude and phase, one may find it difficult to directly use them to define a cost function for the purpose of design optimization. This problem is further compounded by the fact that the magnitudes of the transmitted forces are not necessarily the most important factors that affect the vibration levels on or the sound radiation from the supporting structure.

As a matter of fact, it has long been recognized that a more comprehensive isolation analysis should take into account the impedance characteristics of the sources and/or the supporting structures [1–4]. Power flows from a vibratory machine through isolators into its supporting structure have recently been widely used to assess the effectiveness of a passive or active vibration isolation system

0022-460X/99/290757 + 18 $30.00/0

[5–12]. Prediction of power flows requires the simultaneous determination of the isolator forces acting on and the corresponding responses of the supporting structure. In references [5–7], the impedance behaviors of the supporting structures are represented by simple straight lines when plotted on a log–log scale. The power flows from a spring-supported point mass to a finite beam were studied by Goyder and White [8] with emphasising on when the simple straight line impedance formulae could be adequately used to make frequency-averaged power prediction. Power transmissions from a rigid body, through multiple isolators, to a simple plate and cylindrical shell were investigated in references [9, 10]. Gardonio *et al.* [11, 12] have used a matrix approach to model an active isolation system in which the dynamics of the machine, the isolators and the supporting structure (receiver) are expressed in terms of the point and transfer mobilities or impedances. Use of the total power flow as a cost function was compared with approaches based on the out-of-plane velocities or forces. It has been shown that the control of total power gives the best results under ideal conditions. Sanderson [13] studied the effects of the rotational isolator stiffnesses by considering the power flows between two beams that are connected by one or more isolators in various forms. An error level was used to measure the contributions of the rotational stiffnesses, which is defined as the dB difference in the total power flows calculated with and without including the rotational isolator stiffnesses. It has been demonstrated that the power flows associated with the rotational d.o.f.s should be considered when the normalized (translational to rotational) stiffness ratio is not sufficiently large or the structural wavelength is shorter than the involved beams for the stiffness ratio close to unity. He concluded that the power flows related to the rotational stiffnesses can be either positive or negative and the maximum error levels typically occur at the resonant and anti-resonant frequencies of the beam structures. The importance of the moment excitations to power flows were also discussed in references [14–19].

In this study, a dynamic model is described for vibration isolation systems consisting of a source machine, multiple vibration isolators and a supporting structure. The machine is modeled as a rigid body of six degrees of freedom. Each of the isolators is treated as an assembly of six simple translational and rotational springs and allowed to be inclined at arbitrary angles. The supporting structure is composed of a rectangular plate and a number of reinforcing beams placed in any directions. The equation of motion of such a composite structure is derived from Hamilton's principle and then combined with that of the machine to determine the modal characteristics and vibrations of the whole isolation system, the reaction forces at each isolator, and the power flows into the supporting structure. Numerical examples are presented to examine the power flows under various situations.

2. DYNAMIC DESCRIPTION OF A COMPOSITE ISOLATION SYSTEM

2.1. THE VIBRATION OF THE MACHINE

Consider a generic vibration isolation system consisting of a vibratory machine, several isolators and a supporting structure, as shown in Figure 1. In isolation

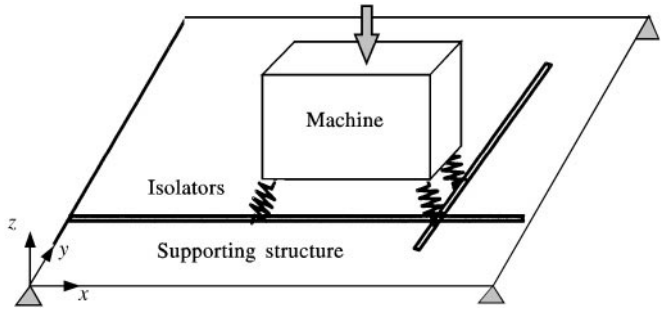

Figure 1. Schematic of a vibration isolation system.

analyses, the machine is often modeled as a 6-d.o.f. rigid body characterized by a mass matrix

$$\mathbf{M} = \begin{bmatrix} m & 0 & 0 & 0 & 0 & 0 \\ 0 & m & 0 & 0 & 0 & 0 \\ 0 & 0 & m & 0 & 0 & 0 \\ 0 & 0 & 0 & I_{xx} & -I_{xy} & -I_{xz} \\ 0 & 0 & 0 & -I_{yx} & I_{yy} & -I_{yz} \\ 0 & 0 & 0 & -I_{zx} & -I_{zy} & I_{zz} \end{bmatrix}. \tag{1}$$

where m is the mass of the machine, and $I_{xx}, I_{yy}, \ldots, I_{yz}$ are the moments and products of the inertia.

The differential equations that govern the motions of the machine can be written as

$$\mathbf{M}\ddot{\mathbf{u}}^{\mathrm{c}} = \mathbf{f}^{\mathrm{m}} + \sum_{i=1}^{N_k} \mathbf{R}_i^{\mathrm{c}}, \tag{2}$$

where $\mathbf{u}^{\mathrm{c}}$ is the displacement vector of the center of gravity (or C.G.) of the machine, $\mathbf{R}_i^{\mathrm{c}}$ is the "localized" load due to the reaction forces at the ith mounting point, $\mathbf{f}^{\mathrm{m}}$ represents the remaining forces acting on the machine, and N_k is the number of isolators.

The reaction forces at the ith isolator can be expressed as

$$\mathbf{R}_i = -\mathbf{K}_i(\mathbf{u}_i - \mathbf{u}_i^0), \tag{3}$$

where $\mathbf{u}_i$ and $\mathbf{u}_i^0$ are, respectively, the displacement vectors at the upper and lower ends of the ith isolator which is represented by an elasticity matrix $\mathbf{K}_i$.

The reaction forces and the displacements at each mounting point can be easily "transformed" to the C.G. of the machine, *via*

$$\mathbf{u}_i = \mathbf{G}_i\mathbf{u}^{\mathrm{c}}, \qquad \mathbf{R}_i^c = \mathbf{G}_i^{\mathrm{T}}\mathbf{R}_i, \tag{4, 5}$$

where

$$\mathbf{G}_i = \begin{bmatrix} 1 & 0 & 0 & 0 & a_z^i & -a_y^i \\ 0 & 1 & 0 & -a_z^i & 0 & a_x^i \\ 0 & 0 & 1 & a_y^i & -a_x^i & 0 \\ 0 & 0 & 0 & 1 & 0 & 0 \\ 0 & 0 & 0 & 0 & 1 & 0 \\ 0 & 0 & 0 & 0 & 0 & 1 \end{bmatrix}. \tag{6}$$

and a_x^i, a_y^i, and a_z^i, are, respectively, the projections onto the x-, y- and z-axis of the distance (vector) from the machine C.G. to the top of the ith isolator.

The isolators will be here considered as an assembly of six simple linear and rotational springs. Assume that p, q and r are the axes of these springs locally defined on the ith isolator. Then its stiffness matrix can be expressed as

$$\mathbf{K}_i = \hat{\mathbf{T}}_i^{\mathrm{T}} \operatorname{diag}(K_i^p, K_i^q, K_i^r, K_i'^p, K_i'^q, K_i'^r) \hat{\mathbf{T}}_i, \tag{7}$$

where diag(.) denotes the diagonal matrix formed from the listed elements, K_i^j and $K_i'^j$ ($j = p, q,$ or r), are, respectively, the linear stiffness in and the rotational stiffness about the j-direction, and

$$\hat{\mathbf{T}}_i = \begin{bmatrix} \mathbf{T}_i & \mathbf{0} \\ \mathbf{0} & \mathbf{T}_i \end{bmatrix} \tag{8}$$

with

$$\mathbf{T}_i = \begin{bmatrix} \lambda_{px}^i & \lambda_{py}^i & \lambda_{pz}^i \\ \lambda_{qx}^i & \lambda_{qy}^i & \lambda_{qz}^i \\ \lambda_{rx}^i & \lambda_{ry}^i & \lambda_{rz}^i \end{bmatrix} \tag{9}$$

being the transformation matrix whose elements are simply the direction cosines of the axes of the springs.

Without loss of generality, the springs, K_i^p, K_i^q, K_i^r, will be defined in such a way that K_i^r, is parallel to the isolator's axis, and K_i^p is (perpendicular to K_i^r and) in the plane which contains K_i^r and the z-axis, as illustrated in Figure 2. As a result, the spatial orientations of the spring can be fully specified in terms of the two spherical angles, ϕ_i and θ_i, and the transformation matrix can be explicitly expressed as

$$\mathbf{T}_i = \begin{bmatrix} \cos\theta_i \cos\phi_i & \cos\theta_i \sin\phi_i & -\sin\theta_i \\ -\sin\phi_i & \cos\phi_i & 0 \\ \sin\theta_i \cos\phi_i & \sin\theta_i \cos\phi_i & \cos\theta_i \end{bmatrix}. \tag{10}$$

Substituting equations (3)–(5) into equation (2) results in

$$\mathbf{K}^{\mathrm{mm}} \mathbf{u}^{\mathrm{c}} + \mathbf{M}^{\mathrm{mm}} \ddot{\mathbf{u}}^{\mathrm{c}} = \mathbf{f}^{\mathrm{m}} + \sum_{i=1}^{N_k} \mathbf{K}_i^{\mathrm{g}} \mathbf{u}_i^0, \tag{11}$$

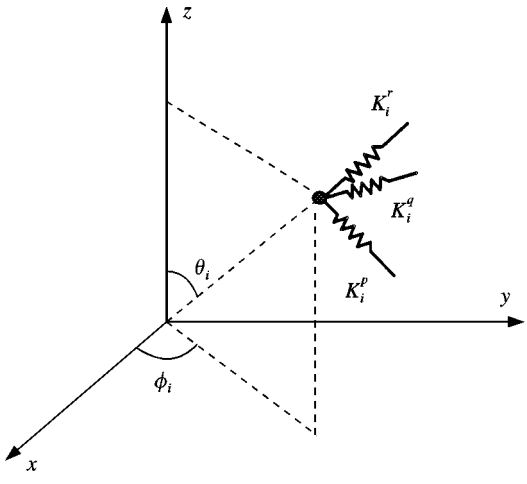

Figure 2. An inclined isolator.

where

$$\mathbf{K}^{\mathrm{mm}} = \sum_{i=1}^{N_k} \mathbf{G}_i^{\mathrm{T}} \mathbf{K}_i \mathbf{G}_i, \qquad \mathbf{K}_i^{\mathrm{g}} = \mathbf{G}_i^{\mathrm{T}} \mathbf{K}_i. \tag{12, 13}$$

In equation (11), the superscript mm is introduced to indicate that these matrices are directly associated with the machine vibration. If the vibrations of the supporting structure are so small that the resulting forces, $\sum_{i=1}^{N_k} \mathbf{K}_i^{\mathrm{g}} \mathbf{u}_i^0$, are negligible as compared with the applied force $\mathbf{f}^{\mathrm{m}}$, equation (11) along can be used to determine the motions of the machine. However, when the vibrations of the supporting structure are significant as happened in many cases, the machine vibrations can no longer be adequately determined without explicitly knowing the motions of the supporting structure at the mounting points. Therefore, the motions of the machine and supporting structure are now coupled together, which requires an additional structural equation for a complete solution.

2.2. THE VIBRATION OF THE SUPPORTING STRUCTURE

The equation of the motion of the supporting structure will be derived by using Hamilton's principle,

$$\delta \int_{t_0}^{t_1} (T - V)\,\mathrm{d}t = 0, \tag{14}$$

where T is the total kinetic energy, V is the total potential energy, and t_0 and t_1 are time limits.

In the current study, the supporting structure is assumed to be a simply supported rectangular plate reinforced by a number of beams with arbitrary lengths and directions. Accordingly, the total kinetic and potential energies can be

expressed as

$$T = T_p + T_b, \qquad V = V_p + V_b + V_f \tag{15, 16}$$

with

$$T_p = \frac{\rho h}{2}\int_0^a\int_0^b \dot{w}^2\,\mathrm{d}x\,\mathrm{d}y, \qquad T_b = \frac{1}{2}\sum_{i=1}^{N_k}\int_0^{L_i}[\rho_i A_i \dot{w}^2 + \rho_i I_i \dot{w}_{x'}^2 + \rho_i J_i \dot{w}_{y'}^2]\,\mathrm{d}x', \tag{17, 18}$$

$$V_p = \frac{D_p}{2}\int_0^a\int_0^b [w_{xx}^2 + w_{yy}^2 + 2\nu w_{xx}w_{yy} + 2(1-\nu)w_{xy}^2]\,\mathrm{d}x\,\mathrm{d}y, \tag{19}$$

$$V_b = \frac{1}{2}\sum_{i=1}^{N_k}\int_0^{L_i}[E_i I_i w_{x'x'}^2 + J_i G_i w_{x'y'}^2]\,\mathrm{d}x', \qquad V_f = -\sum_{i=1}^{N_k}\mathbf{R}_i^{\mathrm{T}}\mathbf{u}_i^0, \tag{20, 21}$$

where $\dot{w} = \partial w/\partial t$, $w_x = \partial w/\partial x$, and $w_{xy} = \partial^2 w/\partial x\,\partial y$; $D_p = Eh^3/12(1-\nu^2)$ is the bending stiffness of a plate of length a, width b and thickness h; E, ν and ρ are, respectively, the Young's modulus, the Poisson ratio and the mass density of the plate; E_i, G_i, ρ_i, L_i, A_i, I_i and J_i are, respectively, the Young's modulus, the shear modulus, the mass density, the length, the cross-sectional area, the area moment of inertia and the torsional constant of the ith beam; and N_b is the total number of reinforcing beams.

Neglecting the in-plane displacements and the drilling rotation of the supporting structure, the displacements of the lower end of the ith isolator can be written as

$$\mathbf{u}_i^0 = \left\{0, 0, w, \frac{\partial w}{\partial y}, -\frac{\partial w}{\partial x}, 0\right\}^{\mathrm{T}}\Bigg|_{x=x_i,\, y=y_i}. \tag{22}$$

In equations (18) and (20), the kinetic and potential energies for each beam are expressed in terms of the local co-ordinates (x', y', z') which are defined such that the x'-axis always lies on the beam and $z' = z$, as shown in Figure 3. The derivatives with respect to the local co-ordinates can be easily determined from

$$\frac{\partial w}{\partial x'} = \frac{\partial w}{\partial x}l_x + \frac{\partial w}{\partial y}l_y, \qquad \frac{\partial w}{\partial y'} = -\frac{\partial w}{\partial x}l_y + \frac{\partial w}{\partial y}l_x, \tag{23, 24}$$

$$\frac{\partial^2 w}{\partial x'^2} = \frac{\partial^2 w}{\partial x^2}l_x^2 + \frac{\partial^2 w}{\partial x\,\partial y}l_x l_y + \frac{\partial^2 w}{\partial y^2}l_y^2, \tag{25}$$

and

$$\frac{\partial^2 w}{\partial x'\,\partial y'} = \left(\frac{\partial^2 w}{\partial y^2} - \frac{\partial^2 w}{\partial x^2}\right)l_x l_y + \frac{\partial^2 w}{\partial x\,\partial y}(l_x^2 - l_y^2), \tag{26}$$

where $l_x = (L_{xe} - L_{xb})/\sqrt{(L_{xe} - L_{xb})^2 + (L_{xe} - L_{yb})^2}$ and $l_y = (L_{ye} - L_{yb})/\sqrt{(L_{xe} - L_{xb})^2 + (L_{xe} - L_{yb})^2}$ are the direction cosines of the beam axis, and L_{xb} and L_{xe} (L_{yb} and L_{ye}) are the x-co-ordinates (y-co-ordinates) of the ends of the beam.

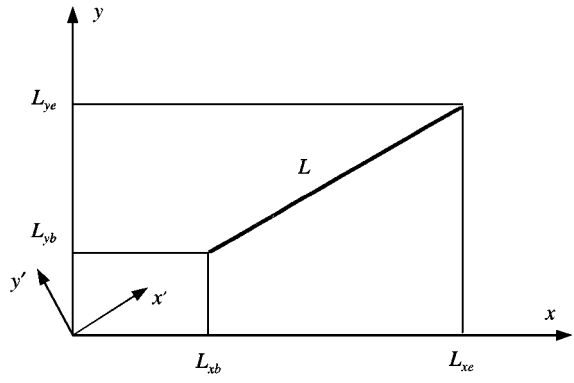

Figure 3. The local co-ordinate system defined on a beam.

Making use of these results, for example, the potential energy corresponding to the bending of the ith beam can be written as

$$\frac{1}{2}\int_0^{L_i} E_i I_i [w_{x'x'}(x')]^2 \,\mathrm{d}x'$$

$$= \frac{1}{2}\int_{L_{xbi}}^{L_{xei}} E_i I_i \left\{ \frac{\partial^2 w[x, L_{ybi} + (l_{yi}/l_{xi})(x - L_{xbi})]}{\partial x^2} l_{xi}^2 \right.$$

$$+ \frac{\partial^2 w[x, L_{ybi} + (l_{yi}/l_{xi})(x - L_{xbi})]}{\partial x \partial y} l_{xi} l_{yi}$$

$$\left. + \frac{\partial^2 w[x, L_{ybi} + (l_{yi}/l_{xi})(x - L_{xbi})]}{\partial^{y2}} l_{yi}^2 \right\}^2 \sqrt{1 + (l_{yi}/l_{xi})^2}\,\mathrm{d}x. \tag{27}$$

The remaining integrals associated with the beams will be calculated in the same manner. For $L_{xbi} - L_{xei}$, the expressions will become much simpler by realizing $(x', y') \equiv (y, -x)$.

Here, the eigenfunctions for the simply supported plate are chosen as the admissible functions for the flexural displacement of the supporting structure, that is,

$$w = \sum_{m=1}^{M} \sum_{n=1}^{N} A_{mn} \varphi_m^a(x) \varphi_n^b(y), \tag{28}$$

where A_{mn} is the expansion coefficient,

$$\varphi_m^a(x) = \sqrt{\frac{2}{a}} \sin k_m^a x, \quad (k_m^a = m\pi/a), \tag{29}$$

and

$$\varphi_n^b(y) = \sqrt{\frac{2}{b}} \sin k_n^b y, \quad (k_n^b = n\pi/b). \tag{30}$$

Substitution of equations (15)–(30) into equation (14) results in

$$(\mathbf{K}^{ss} - \omega^2 \mathbf{M}^{ss})\mathbf{A} - \mathbf{K}^{sm}\mathbf{u}_c = \mathbf{f}^s, \tag{31}$$

where

$$\mathbf{A} = \{A_{11}, A_{12}, \ldots, A_{MN}\}^T, \qquad \mathbf{K}^{sm} = \sum_{i=1}^{N_k} \{\mathbf{D}^i_{11}, \mathbf{D}^i_{12}, \ldots, \mathbf{D}^i_{MN}\}^T \mathbf{K}_i^{g^T}, \tag{32, 33}$$

$$\mathbf{D}^i_{mn} = \{0, 0, \varphi^a_m(x,y)\varphi^b_n(x,y), k^b_n \varphi^a_m(x,y)\varphi^b_{yn}(x,y), -k^a_m \varphi^a_{xm}(x,y)\varphi^b_n(x,y), 0\}^T|_{x=x_i, y=y_i}, \tag{34}$$

$$\varphi^a_{xm}(x) = \sqrt{2/a}\cos k^a_m x, \qquad \varphi^b_{yn}(y) = \sqrt{2/b}\cos k^b_n y, \tag{35, 36}$$

and $\mathbf{K}^{ss}$ and $\mathbf{M}^{ss}$ are, respectively, the stiffness and mass matrices whose expressions are given in Appendix A

2.3. COUPLED MOTIONS AND POWER FLOWS

In light of equations (22) and (28), equation (11) can be rewritten as

$$\mathbf{K}^{mm}\mathbf{u}^c + \mathbf{M}^{mm}\ddot{\mathbf{u}}^c = \mathbf{f}^m + \mathbf{K}^{ms}\mathbf{A}, \tag{37}$$

where

$$\mathbf{K}^{ms} = \mathbf{K}^{sm^T}. \tag{38}$$

Combining equations (31) and (37) leads to

$$\begin{bmatrix} \mathbf{K}^{ss} & -\mathbf{K}^{sm} \\ -\mathbf{K}^{ms} & \mathbf{K}^{mm} \end{bmatrix} \begin{Bmatrix} \mathbf{A} \\ \mathbf{u}^c \end{Bmatrix} - \omega^2 \begin{bmatrix} \mathbf{M}^{ss} & 0 \\ 0 & \mathbf{M}^{mm} \end{bmatrix} \begin{Bmatrix} \mathbf{A} \\ \mathbf{u}^c \end{Bmatrix} = \begin{Bmatrix} \mathbf{0} \\ \mathbf{f}^m \end{Bmatrix}. \tag{39}$$

The vibrations of the machine and the supporting structure can now be obtained simultaneously from equation (39). Setting the external forces $\mathbf{f}^m$ to zero, equation (39) reduces to a standard characteristic equation from which the modal properties of the composite system can be directly determined. Because the responses are often desired at a large number of frequency steps, the modal superposition technique is here used to solve equation (39).

The power flow, say, through the jth isolator into the supporting structure can be obtained from

$$P_j = \tfrac{1}{2}\Re\{\mathrm{i}\omega \mathbf{R}_j^T \, conj(\mathbf{u}_j^0)\}, \tag{40}$$

where $\Re\{.\}$ and $conj(.)$ denote the real part and complex conjugate of a complex quantity, respectively.

The total or net power flow from the machine into the supporting structure is the sum of the power flows through each of the isolators, namely,

$$P_t = \sum_j^{N_k} P_j = \frac{1}{2}\sum_j^{N_k} \Re\{\mathrm{i}\omega \mathbf{R}_j^T \, conj(\mathbf{u}_j^0)\}. \tag{41}$$

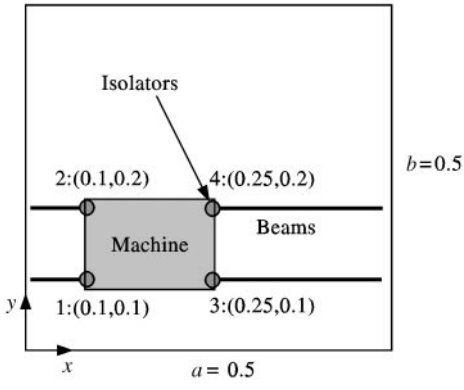

Figure 4. The positions of the isolators and beams.

The total power flow is clearly a function of those variables that are used to specify the physical and geometrical properties of the machine, the supporting structure, and the vibration isolators. Therefore, it can be conveniently used as a cost function to be minimized in a vibration isolation design optimization.

In the above discussion, the characteristics of the isolators have been simply represented by a diagonal stiffness matrix. A more general relationship between the isolator end forces and displacements can be expressed as

$$\begin{Bmatrix} \mathbf{R}_i \\ \mathbf{R}_i^0 \end{Bmatrix} = \begin{bmatrix} \mathbf{K}_i^{11} & \mathbf{K}_i^{12} \\ \mathbf{K}_i^{21} & \mathbf{K}_i^{22} \end{bmatrix} \begin{Bmatrix} \mathbf{u}_i \\ \mathbf{u}_i^0 \end{Bmatrix}, \tag{42}$$

where $\mathbf{R}_i^0$ denotes the reaction forces at the lower end of the ith isolator and $\mathbf{K}_i^{jk}$ ($j, k = 1$ or 2) generally represents a full 6×6 stiffness matrix. Although the determination of these stiffness matrices may be an issue of practical concern, one may find it is not difficult to directly incorporate this modification, equation (42), into the above expressions.

3. RESULTS AND DISCUSSIONS

For demonstration, consider a machine mounted on a $0{\cdot}5\,\mathrm{m} \times 0{\cdot}5\,\mathrm{m} \times 0{\cdot}002\,\mathrm{m}$ simply supported plate that is reinforced by two identical beams in the x-direction, as illustrated in Figure 4. The plate and beams are made of steel ($E = 2{\cdot}07 \times 10^{11}\,\mathrm{N\,m^{-2}}$, $\nu = 0{\cdot}3$ and $\rho = 7800\,\mathrm{kg\,m^{-3}}$). The other related parameters for the machine, the isolators and the beams are listed in Table 1. A uniform modal damping ratio, 0·02, is assumed in the following calculations. An extra 2% hysteretic damping is added to the isolators.

3.1. THE MODES OF THE COMPOSITE ISOLATION SYSTEM

As a rule of thumb in a machine isolation design, the lowest natural frequencies of the isolation system should be sufficiently lower than or distanced from the

TABLE 1
The properties of the machine, isolators and beams

Isolators		Machine		Beams	
$K_p = K_q$	$2{\cdot}5 \times 10^6$ N m^{-1}	m	30 kg	A	5×10^{-5} m^2
K_r	10^7 N m^{-1}	I_{xx}	0·0244 kg m^2	I	10^{-10} m^4
$K'_p = K'^q$	$2{\cdot}5 \times 10^4$ N m rad^{-1}	I_{yy}	0·0369 kg m^2	J	2×10^{-10} m^4
K'_r	10^5 N m rad^{-1}	I_{zz}	0·0325 kg m^2	L	0·5 m

TABLE 2
The lowest natural frequencies (in Hz) of the machine, the supporting structure, and the combined isolation system

Mode number	The Machine on the isolators	The supporting structure alone	The whole isolation system
1	81·7	41·2	12·9
2	85·2	96·1	23·5
3	161·2	111·0	29·2
4	162·1	164·2	97·5
5	183·8	187·4	105·2
6	193·7	220·5	112·2
7	—	254·6	142·2
8	—	284·9	193·7
9	—	318·9	197·9
10	—	364·5	244·8

fundamental excitation frequency and its first few multiples. However, the modal parameters independently predicted for the unloaded supporting structure or the machine mounted on a set of grounded isolators can be meaningfully modified when the interaction of the machine and the supporting structure is taken into account. To study the effects, Table 2 compares the lowest natural frequencies for the unloaded supporting structure, the machine resting on the grounded isolators, and the whole combined isolation system. Of the six machine modes, only the yawing mode at 193·7 Hz is not affected by the inclusion of the supporting structure. The results clearly indicate that the effects of the coupling between the machine and the supporting structure need to be considered for an accurate prediction.

Given in Figure 5 are four selected mode shapes for the loaded (supporting) structure. In the first mode, the presence of the machine is simply manifested as a mass loading. The machine's influences cannot be so easily characterized for the other structural modes. However, the strong couplings between the motions of the machine and the supporting structure are primarily limited to five of the first six modes (except for the fourth mode). For the higher order modes, the motions of the

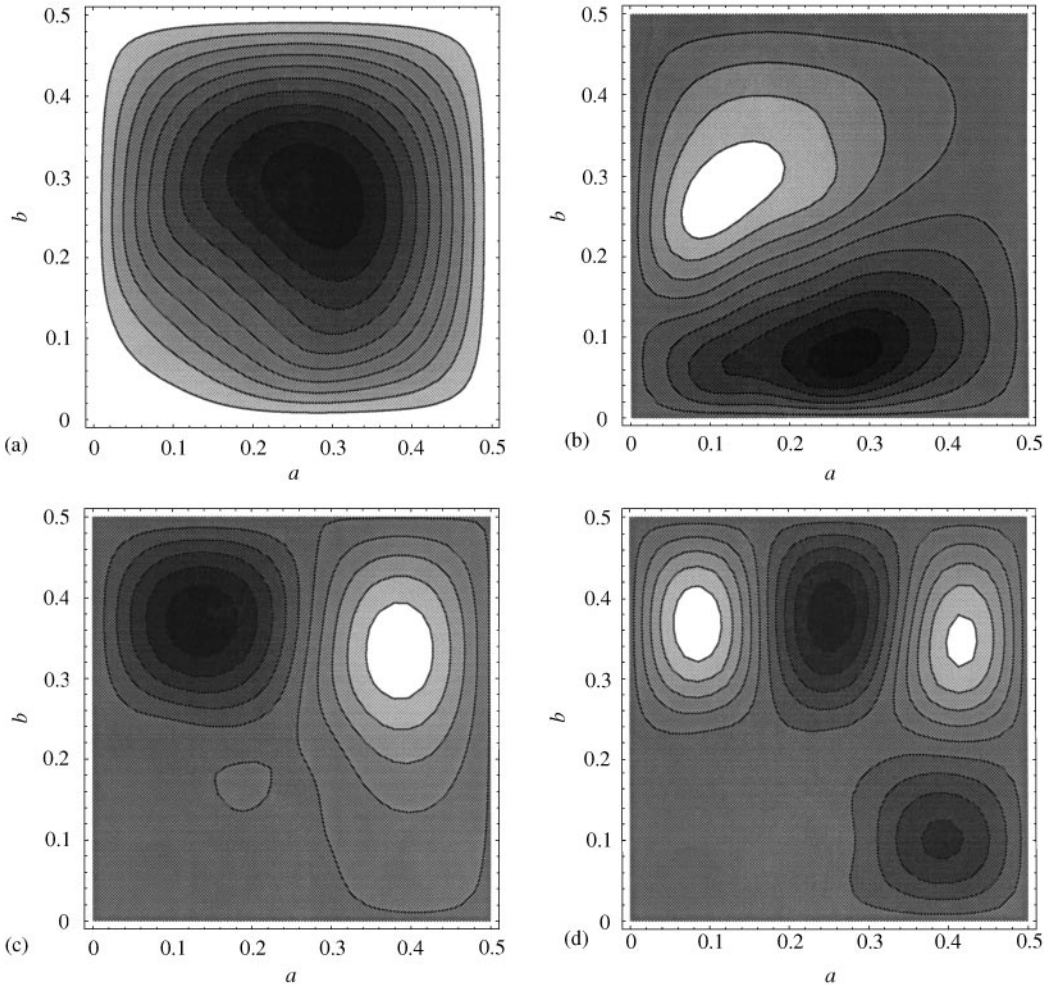

Figure 5. Four of the lower structural modes: (a) $f_1 = 12{\cdot}9$ Hz, (b) $f_2 = 23{\cdot}5$ Hz, (c) $f_7 = 142{\cdot}2$ Hz, and (d) $f_{10} = 244{\cdot}8$ Hz.

machine become insignificant and the structural modes such as the last two in Figure 5 can be essentially obtained by assuming the isolators are grounded at the machine ends.

In the above modal analysis, 64 eigenfunctions ($M = N = 8$) have been used in equation (28), allowing a total of 70 modes (for the whole isolation system) to be included in the following power flow calculations).

3.2. THE POWER FLOWS INTO THE SUPPORTING STRUCTURE

Assume that a point force, $F_x = 1$ N, is applied to the machine C.G. in the x-direction. Figure 6 shows the total power flow into the supporting structure versus the sum of the vertical reaction forces at each isolator location. The force and

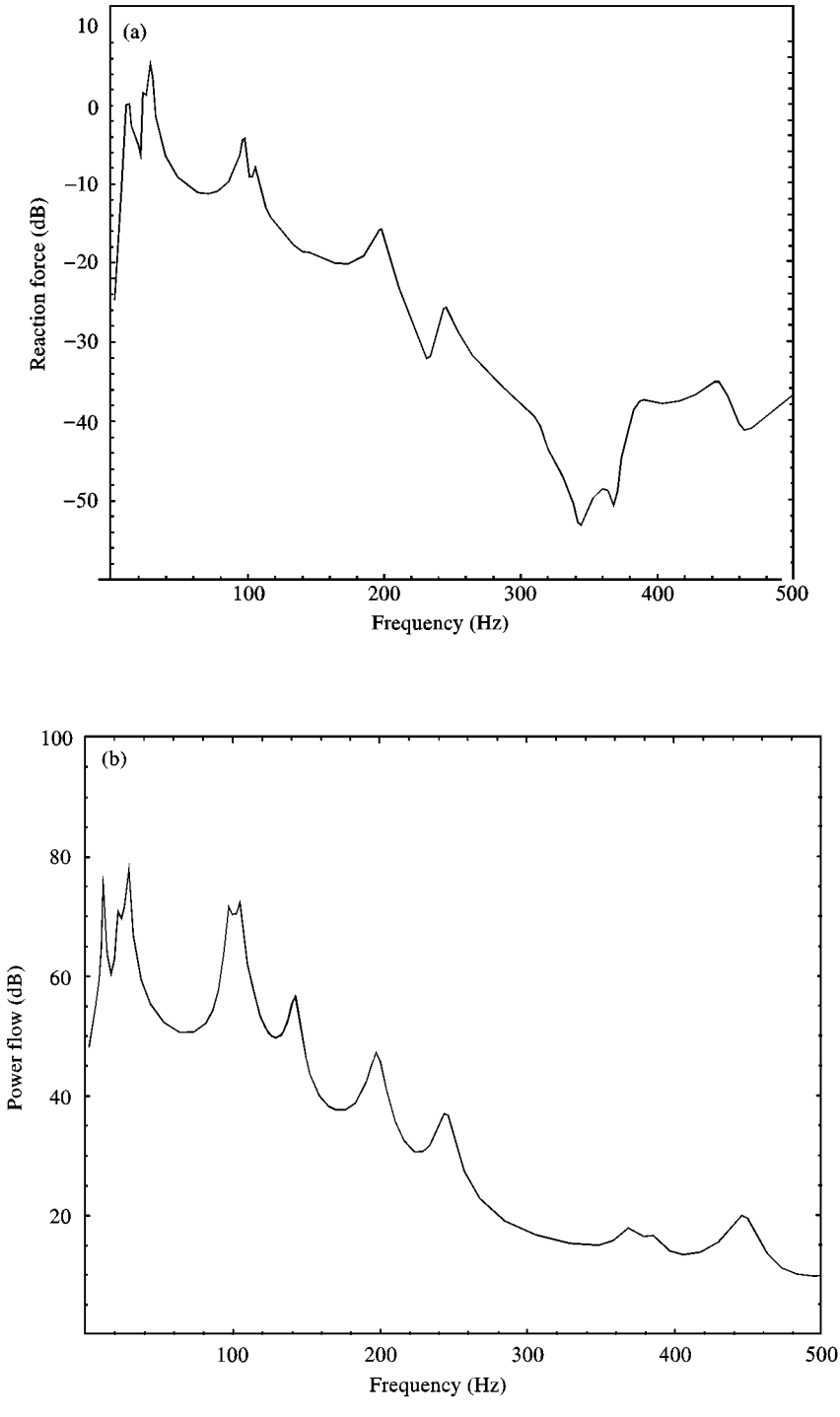

Figure 6. (a) The total vertical reaction force in dB (reference 1 N) versus (b) the total power flow in dB (reference 10^{-12} W); $F_x = 1$ N.

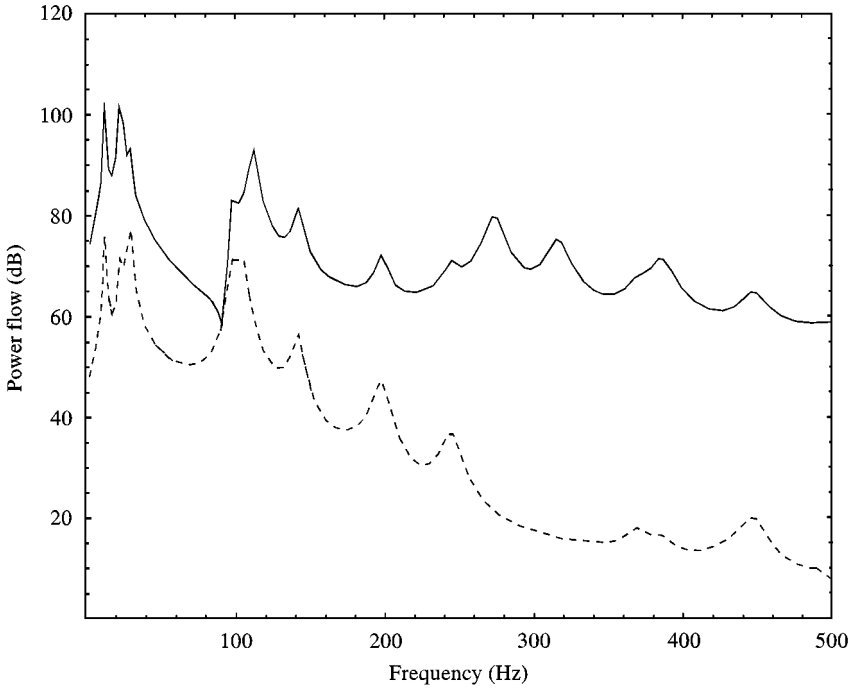

Figure 7. The total power flows: ——, $M_x = 1$ N m; - - - - - -, $F_x = 1$ N.

power predictions are noticeably different, especially at high frequencies. For instance, the force analysis is unable to produce the sixth peak at 142 Hz (corresponding to the seventh mode) on the power curve, nor does it predict the same trend toward the end of the frequency range. However, that the use of the total reaction force to assess the isolation efficiency may be problematic at high frequencies should not come as a surprise: when the distances between the isolators become comparable to or longer than the wavelengths of the structural waves, the "total reaction force" may no longer be a meaningful term.

Now consider a different loading case: the machine is subjected to a moment about the x-axis, $M_x = 1$ N m. The total power flow is compared in Figure 7 with that for the previous case. It is seen that the power flow curve tends to be flat for the moment excitation. This is essentially consistent with the existing knowledge about the (frequency-averaged) response characteristics of plates or beams under a moment excitation. Intuitively, the gross effect of the reaction forces on the supporting structure should be moment-like for this loading case. However, instead of increasing with frequency as expected, the power flow curve is roughly constant here. This may be due to the fact that the unity moment applied has been partially "absorbed" by the machine (inertia) at a speed of about 6-dB per octave.

The power flows through each isolator are also of interest. Even though the total power flow is typically from the source machine to the supporting structure, those through each individual isolator may not necessarily be equal or occur in the same direction. Figure 8 details the power flows through the two front (labeled 1 and 3 in

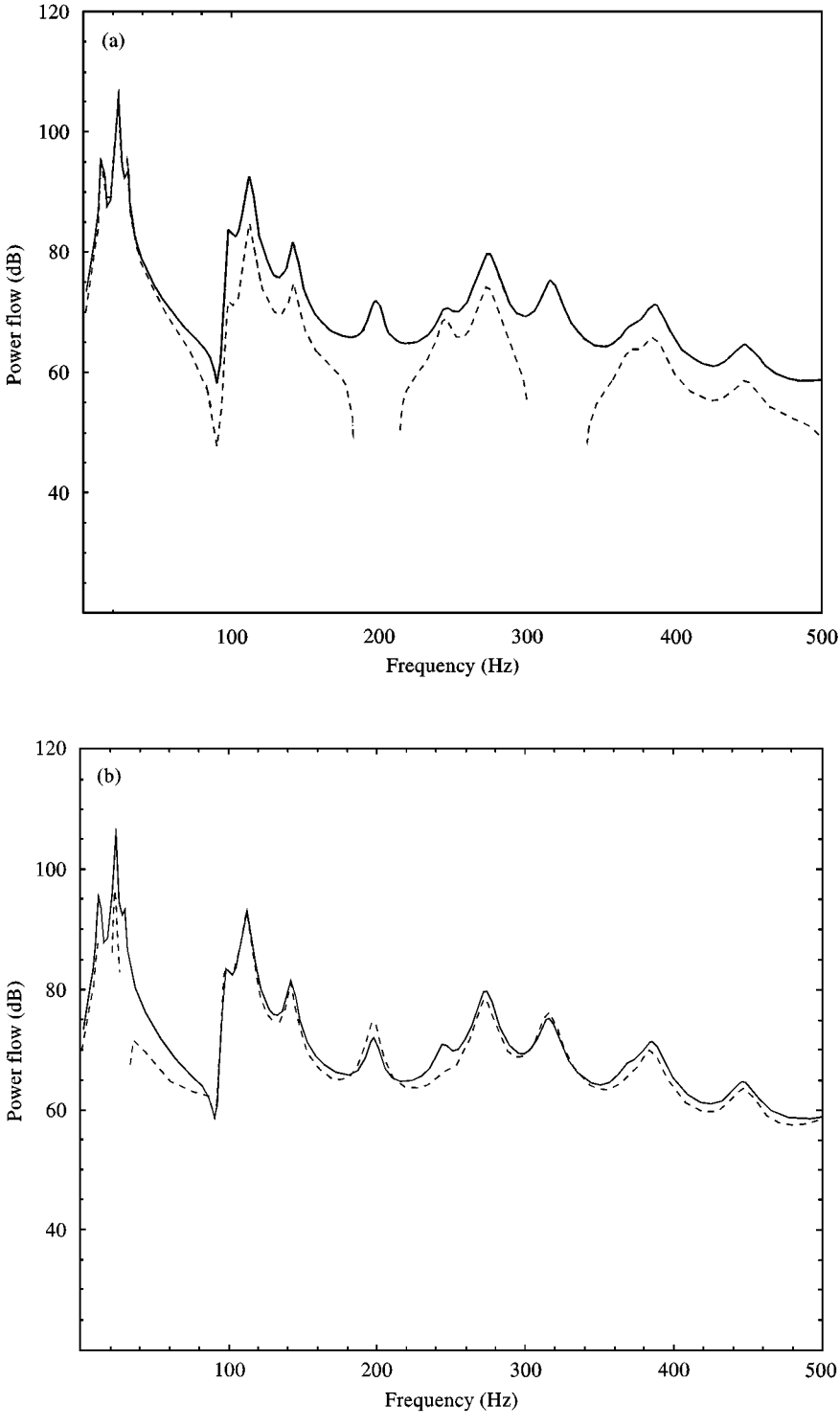

Figure 8. The power flows through: (a) ——, the four isolators; - - - - - , the two front isolators; (b) - - - - - , the two rear isolators; $M_x = 1$.

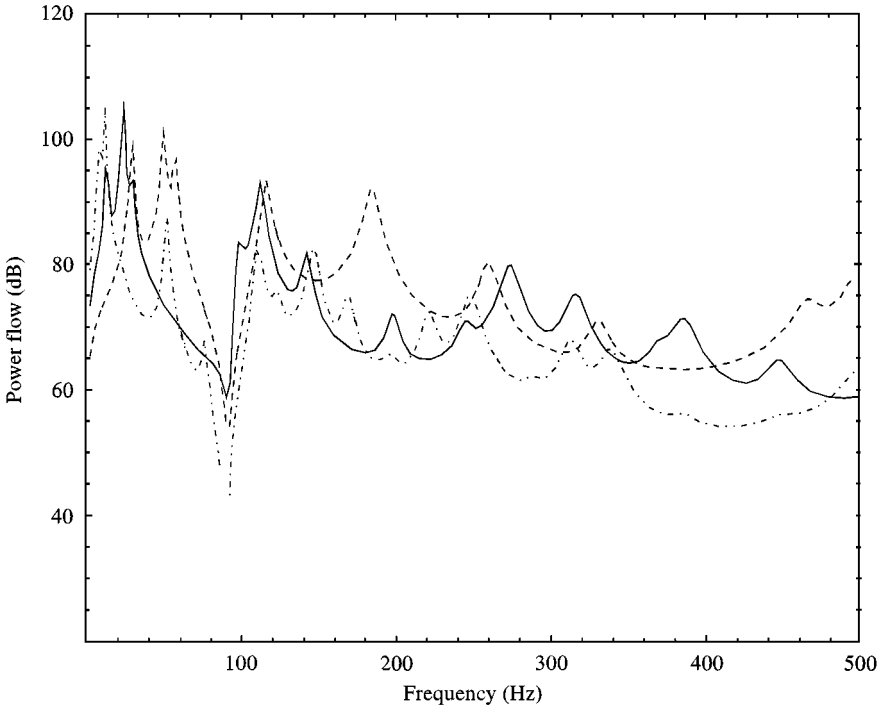

Figure 9. The total power flows: ——, original plate; - - - - - , 0·004 m plate; and – · – · – · – · , 0·001 m plate; $M_x = 1$.

Figure 4) and two rear isolators (labeled 2 and 4). Before the first natural frequency, the amounts of power flows through each group are basically equal. Near the first three peaks, the two front isolators dominate the power flow into the supporting structure. In the rest of the frequency range, the power transmission is primarily through the two rear isolators. The missing parts of the curves (say, near 200 Hz on the curve for the front isolators) indicate a negative power flow (from the supporting structure to the machine). The amounts of the negative power flows can be read from the surpluses on the other curve at the corresponding frequencies.

Power flows are functions of the variables used to either specify the properties of the involved components (the machine, the isolators and the supporting structure) or describe the way in that the whole isolation system is assembled. As an example, a simple structural modification will be considered here: changing the plate thickness from 0·002 to 0·001 and 0·004 m. The total power flow curves are compared in Figure 9 for these three different plates. Realizing that the curves in Figure 9 actually represent the power transmission characteristics of the isolation systems, a quantitative comparison of their overall isolation efficiencies cannot be made without explicitly knowing the spectra of the actual loads acting on the machine. However, a qualitative comparison may still be possible. For instance, Figure 9 shows that the 0·001 m plate outperforms the 0·004 m one almost in the whole frequency range. The effects of modifying other design variables can be evaluated in the same manner.

4. CONCLUDING REMARKS

A dynamic model has been described for determination of the vibrations of the power flows between a vibratory machine and its supporting structure. Because the interaction of the machine and the supporting structure has been taken into account, the modal parameters of the whole isolation system can be accurately obtained which are usually found quite different from those independently determined for the components. Typically, only the several lowest modes exhibit a strong coupling between the motions of the machine and the supporting structure and the remaining modes may be simply determined as if the isolators were grounded at the machine ends.

In comparison with the reaction forces, power flows are a more manageable and perhaps more meaningful measure of the effectiveness of a vibration isolation systems, especially at high frequencies. The power flows as a physical quantity may also carry more information on how to improve an isolation design. When a machine is mounted on multiple isolators, the amounts and the directions of the power flows through each isolator can be substantially different and vary with frequency. Although the power flow analysis involves solving a more complicated dynamic problem, the extra effort may be worthwhile with regard to the aforementioned benefits. Furthermore, in view of the relative ease of specifying the machine loads, such a combined analysis can effectively avoid the difficulties, which may otherwise be encountered in an isolated structural analysis, associated with determining the loads actually applied on the supporting structure.

REFERENCES

1. J. I. Soliman and M. G. Hallam 1968 *Journal of Sound and Vibration* **8**, 329–351. Vibration isolation between non-rigid machines and non-rigid foundations.
2. E. E. Ungar and C. W. Dietrich 1966 *Journal of Sound and Vibration* **4**, 224–241. High frequency vibration isolation.
3. A. O. Sykes 1960 *Noise Control* **6**, 23–28. Isolation of vibration: when machine and foundation are resilient and when wave effects occur in the mount.
4. J. L. Soliman and M. G. Hallam 1968 *Journal of Sound and Vibration* **8**, 329–351. Vibration isolation between non-rigid machines and non-rigid foundations.
5. H. G. D. Goyder and R. G. White 1980 *Journal of Sound and Vibration* **68**, 59–75. Vibrational power flow from machines into built-up structures, Part I: Introduction and approximate analyses of beam and plate-like foundations.
6. H. G. D. Goyder and R. G. White 1980 *Journal of Sound and Vibration* **68**, 77–96. Vibrational power flow from machines into built-up structures, Part II: Wave propagation and power flow in beam-stiffened plates.
7. H. G. D. Goyder and R. G. White 1980 *Journal of Sound and Vibration* **68**, 97–117. Vibrational power flow from machines into built-up structures, Part III: Power flow through isolation systems.
8. R. J. Pinnington and R. G. White 1981 *Journal of Sound and Vibration* **68**, 179–197. Power flow through machine isolation to resonant and non-resonant beams.
9. J. Pan, J. Q. Pan and C. H. Hansen 1992 *Journal of the Acoustical Society of America* **92**, 895–907. Total power flow from a vibrating rigid body to a thin panel through multiple elastic mounts.
10. C. Q. Howard, J. Q. Pan and C. H. Hansen 1997 *Journal of the Acoustical Society of America* **101**, 1479–1491. Power transmission from a vibrating body to a circular cylindrical shell through active elastic isolators.

11. P. GARDONIO, S. J. ELLIOTT and R. J. PINNINGTON 1997 *Journal of Sound and Vibration* **207**, 61–93. Active isolation of structural vibration on a multiple-degree-of-freedom system, part I: the dynamics of the system.
12. P. GARDONIO, S. J. ELLIOTT and R. J. PINNINGTON 1997 *Journal of Sound and Vibration* **207**, 95–121. Active isolation of structural vibration on a multiple-degree-of-freedom system, part II: effectiveness of active control strategies.
13. M. A. SANDERSON 1996 *Journal of Sound and Vibration* **198**, 171–191. Vibration isolation: moments and rotations included.
14. B. A. T. PETERSSON 1993 *Journal of Sound and Vibration* **160**, 43–66. Structural acoustic power transmission by point moment and force excitation, part I: beam- and frame-like structures.
15. B. A. T. PETERSSON 1993 *Journal of Sound and Vibration* **160**, 67–91. Structural acoustic power transmission by point moment and force excitation, part I: plate-like structures.
16. Y. K. KOH and R. G. WHITE 1996 *Journal of Sound and Vibration* **196**, 469–493. Analysis and control of vibrational power transmission to machinery supporting structures subjected to a multi-excitation system, part I: driving point mobility matrix of beam and rectangular plates.
17. Y. K. KOH and R. G. WHITE 1996 *Journal of Sound and Vibration* **196**, 495–508. Analysis and control of vibrational power transmission to machinery supporting structures subjected to a multi-excitation system, part II: vibrational power analysis and control schemes.
18. Y. K. KOH and R. G. WHITE 1996 *Journal of Sound and Vibration* **196**, 509–522. Analysis and control of vibrational power transmission to machinery supporting structures subjected to a multi-excitation system, part III: vibrational power cancellation and control experiments.
19. B. A. T. PETERSSON and B. M. GIBBS *Journal of Sound and Vibration* **168**, 157–176. Use of the source descriptor concept in studies of multi-point and multi- directional vibrational sources.

APPENDIX A: ELEMENTS OF THE STIFFNESS AND MASS MATRICES

The detailed expressions of the stiffness and mass matrices in equation (31) are given as follows:

$$
\begin{aligned}
K^{pp}_{mn,m'n'} = {} & \rho h \omega^2_{mn} \delta_{mm'} \delta_{nn'} + \sum_{i=1}^{N_k} (\mathbf{D}^{\mathrm{i}}_{\mathrm{mn}})^{\mathrm{T}} \mathbf{K}_{\mathrm{i}} \mathbf{D}^{\mathrm{i}}_{\mathrm{m'n'}} \\
& + \sum_{i}^{N_b} \Phi^{i}_{mn,m'n'} \{ E_i I_i [((k^a_{m'} l_{xi})^2 + (k^b_{n'} l_{yi})^2)((k^a_m l_{xi})^2 + (k^b_n l_{yi})^2)] \\
& + G_i J_i [((k^a_{m'})^2 + (k^b_{n'})^2)((k^a_m)^2 - (k^b_n)^2) l^2_{xi} l^2_{yi}] \} \\
& - \sum_{i}^{N_b} \Phi'^{i}_{mn,m'n'} \{ 2 E_i I_i k^a_m k^b_n l_{yi} l_{xi} [(k^a_{m'} l_{xi})^2 + (k^b_{n'} l_{yi})^2] \\
& + G_i J_i k^a_m k^b_n [(k^b_{n'})^2 - (k^a_{m'})^2] l_{xi} l_{yi} (l^2_{xi} - l^2_{yi}) \} \\
& - \sum_{i}^{N_b} \Phi'^{i}_{m'n',mn} \{ 2 E_i I_i k^a_{m'} k^b_{n'} l_{yi} l_{xi} [(k^a_m l_{xi})^2 + (k^b_n l_{yi})^2] \\
& + G_i J_i k^a_{m'} k^b_{n'} [(k^b_n)^2 - (k^a_m)^2] l_{xi} l_{yi} (l^2_{xi} - l^2_{yi}) \} \\
& + \sum_{i}^{N_b} \Phi''^{,i}_{mn,m'n'} k^a_m k^a_{m'} k^b_n k^b_{n'} \{ 4 E_i I_i l^2_{yi} l^2_{xi} + G_i J_i (l^2_{xi} - l^2_{yi})^2 \} \qquad \text{(A1)}
\end{aligned}
$$

and

$$M^{pp}_{mn,m'n'} = \delta_{mm'}\delta_{mn'}\rho h + \sum_i^{N_b} \Phi_{mn,m'n'}\rho_i S_i + \sum_i^{N_b} \Phi^{xi}_{mn,m'n'}\rho_i k^a_{m'} k^a_m \{I_i l^2_{xi} + J_i l^2_{yi}\} + \sum_i^{N_b} \Phi^{yi}_{mn,m'n'}\rho_i k^b_{n'} k^b_n \{I_i l^2_{yi} + J_i l^2_{xi}\} + \sum_i^{N_b} \Phi^{xyi}_{mn,m'n'}\rho_i k^a_m k^b_{n'} l_{yi} l_{xi}\{I_i - J_i\} + \sum_i^{N_b} \Phi^{xyi}_{m'n',mn}\rho_i k^a_{m'} k^b_n l_{yi} l_{xi}\{I_i - J_i\}, \tag{A2}$$

where

$$\Phi^{i}_{mn,m'n'} = \int_{L_{xbi}}^{L_{xei}} \{\varphi^a_m(x)\varphi^a_{m'}(x)\varphi^b_n(y)\varphi^b_{n'}(y)\}|_{y=L_{ybi}+(l_{yi}/l_{xi})(x-L_{xbi})}\sqrt{1+(l_{yi}/l_{xi})^2}\,dx, \tag{A3}$$

$$\Phi'^{i}_{mn,m'n'} = \int_{L_{xbi}}^{L_{xei}} \{\varphi^a_{xm}(x)\varphi^b_{yn}(y)\varphi^a_{m'}(x)\varphi^b_{n'}(y)\}|_{y=L_{ybi}+(l_{yi}/l_{xi})(x-L_{xbi})}\sqrt{1+(l_{yi}/l_{xi})^2}\,dx, \tag{A4}$$

$$\Phi''^{,i}_{mn,m'n'} = \int_{L_{xbi}}^{L_{xei}} \{\varphi^a_{xm}(x)\varphi^a_{xm'}(x)\varphi^b_{yn}(y)\varphi^b_{yn'}(y)\}|_{y=L_{ybi}+(l_{yi}/l_{xi})(x-L_{xbi})}\sqrt{1+(l_{yi}/l_{xi})^2}\,dx, \tag{A5}$$

$$\Phi^{xi}_{mn,m'n'} = \int_{L_{xbi}}^{L_{xei}} \{\varphi^a_{xm}(x)\varphi^b_n(y)\varphi^a_{xm'}(x)\varphi^b_{n'}(y)\}|_{y=L_{ybi}+(l_{yi}/l_{xi})(x-L_{xbi})}\sqrt{1+(l_{yi}/l_{xi})^2}\,dx, \tag{A6}$$

$$\Phi^{yi}_{mn,m'n'} = \int_{L_{xbi}}^{L_{xei}} \{\varphi^a_m(x)\varphi^b_{yn}(y)\varphi^a_{m'}(x)\varphi^b_{yn'}(y)\}|_{y=L_{ybi}+(l_{yi}/l_{xi})(x-L_{xbi})}\sqrt{1+(l_{yi}/l_{xi})^2}\,dx, \tag{A7}$$

and

$$\Phi^{xyi}_{mn,m'n'} = \int_{L_{xbi}}^{L_{xei}} \{\varphi^a_{xm}(x)\varphi^b_n(y)\varphi^a_{m'}(x)\varphi^b_{yn'}(y)\}|_{y=L_{ybi}+(l_{yi}/l_{xi})(x-L_{xbi})}\sqrt{1+(l_{yi}/l_{xi})^2}\,dx. \tag{A8}$$